SAND2019-6451C

ILASS-Americas 30th Annual Conference on Liquid Atomization and Spray Systems, Tempe, AZ, May 2019

The influence of ambient conditions and fuel type on gasoline spray plume direction

J. Hwang
Combustion Research Facility
Sandia National Laboratories
Livermore, CA 94550 USA

L. Weiss
Institute of Engineering Thermodynamics
FAU Erlangen-Nuremberg
Erlangen, 91058 Germany
School of Advanced Optical Technologies (SAOT)
FAU Erlangen-Nuremberg
Erlangen, 91052 Germany

L. M. Pickett[*], and S. A. Skeen
Combustion Research Facility
Sandia National Laboratories
Livermore, CA 94550 USA

Abstract

This study investigated the spray behavior of iso-octane, a multi-component surrogate with diisobutylene, and a multi-component fuel with olefin molecular structure. Fuel was injected using Engine Combustion Network (ECN) spray G injector into a continuous flow spray vessel under ECN G2 flash boiling, G3 early injection, and G3HT (G3 with 393 K ambient temperature) conditions. High-speed extinction and Mie-scattering imaging were performed for many injections at different injector rotations, followed by optical property analysis and tomographic reconstruction to identify the 3-D liquid volume fraction distribution and plume direction evolution. Experimental results showed that the expected higher evaporation rate associated with the G3 elevated temperature condition resulted in a shorter liquid axial and radial penetration length compared to the G2 and G3 (baseline) conditions. Compared to the G3 condition, the G2 condition had a narrower liquid plume width but a longer axial liquid penetration despite flash boiling operation. Planar slices, available from the tomographically reconstructed extinction data, confirmed greater plume interaction for the flash boiling condition with an approximately 4° smaller plume direction angle relative to the nozzle drill angle. In terms of fuel, the olefinic fuel, which has a broader distillation curve exhibited the strongest spray plume collapse, but also the longest time for evaporation.

---

[*] Corresponding author: LMPicke@sandia.gov

Sandia National Laboratories is a multimission laboratory managed and operated by National Technology & Engineering Solutions of Sandia, LLC, a wholly owned subsidiary of Honeywell International Inc., for the U.S. Department of Energy's National Nuclear Security Administration under contract DE-NA0003525.

Introduction

Gasoline direct injection (GDI) engines have been adopted by the automotive industry over the past few years. Different from conventional port fuel injection (PFI) engines, GDI engines inject the fuel directly into the combustion chamber. This results in the ability to have a higher compression ratio and more advanced spark timing. These improvements are thanks to the charge cooling effect which mitigates knocking tendency. Hence, GDI engines provide great potential to achieve not only high fuel efficiency, but also low emission levels compared to PFI engines. A combination of direct fuel injection with advanced engine technologies such as high pressure injection, multiple injection strategies, exhaust gas recirculation (EGR) and enhanced air utilization by swirl or tumble motion enable GDI engines to be operated under lean conditions [1-4]. Furthermore, advanced combustion concepts such as low temperature gasoline combustion (LTGC) and spark controlled compression ignition (SPCCI) have been considered as next generation GDI engine technologies [5-6]. These concepts utilize early fuel injection during the intake stroke to form a homogeneous air-fuel mixture. These are followed by late injections near top dead center (TDC) to create a stratified charge near the spark plug. For this technology to succeed, spray control is of upmost importance. Inappropriate injection parameters and fuel induce fuel impingement on the cylinder wall and result in a large amount of particulate matter (PM) emissions [7]. Thus understanding plume direction under various ambient conditions and fuels is crucial to be able to improve combustion and emission characteristics in GDI engines.

One of the interesting features in a gasoline spray can be seen under flash boiling conditions. Flash-boiling occurs at throttled early injection conditions when ambient pressure is lower than the saturation pressure. Rapid changes in temperature and the velocity field are accompanied by a bulk conversion fuel from liquid to vapor. Common observations under flash-boiling condition are shorter liquid penetration length, enhanced atomization, lower mixture temperature, and large recirculating vortex closer to injector tip [8-10]. Different from non-flashing condition where the Reynolds number (*Re*) and Weber number (*We*) represent spray characteristics, ambient pressure to saturation pressure ratios (P_s/P_a) have dominant impact on spray process under flash-boiling condition. As the pressure ratio decreases, plume width gets wider because of the enhanced evaporation and diffusion along the radial direction. The momentum transfer from spray to ambient air incases so velocity field around the spray plume also gets larger [11]. The strong plume-to-plume interactions occur when the pressure ratio is lower than 0.3 [12]. At this moment, a vortex core moves upstream towards the injector and a strong momentum of recirculated air pushes the plumes into the center region. Contacting plumes block air entrainment into the core area causing the spray collapse to be accelerated by a larger pressure difference between center of the spray and ambient air. Based on the phase Doppler interferometry (PDI) measurement, the air entrainment stopped and reverse motion was detected before the plume collapse [13]. Flash-boiling process alters plume direction angle and affects mixture formation in the combustion chamber. Under flare flash-boiling conditions, the injection produces a longer liquid penetration length than a non-flashing condition so wall wetting by spray impingement needs to be carefully examined.

Meanwhile, fuel properties such as distillation characteristics, heat of vaporization, and vapor pressure also affect plume direction and mixture formation. Previous studies showed that longer liquid penetration lengths were found with fuels which have higher heat of evaporation [14-15]. This results are most likely the evaporation rate of spray with higher latent heat got slower than other fuels due to lower temperature field by charge cooling effect. Charge cooling is typically preferred in engine combustion, however, excessive cooling induces emission deterioration. This phenomenon can be seen in an engine experiment where ethanol (high latent heat) showed deteriorated particulate number (PN) emissions when compared to a conventional gasoline fuel due to wall wetting by longer liquid penetration length [16]. This implies that an implementation of a multiple injection strategy is needed to prevent pool fire, but to take advantage of the charge cooling effect. A fuel with a higher vapor pressure, for example propane, showed vigorous flash-boiling compared to other fuels [17]. The propane spray could not maintain its separate plumes and completely collapsed into one spray showing much longer liquid penetration length than n-hexane and iso-ocatne sprays. Complete plume collapse not only restrict air-fuel mixing by limited air utilization but also cause fuel wetting on the cylinder wall or piston bowl. In terms of spray residual time, it showed similar order with distillation characteristics [18]. Heavy components in the fuel resisted to be evaporated and this is resulted in a longer residual time. The longer residual time of liquid fuel is also needs to be avoided because it can create wetting on a moving piston.

A variety of non-intrusive diagnostics have been applied to identify plume direction. Laser diagnostics were widely employed because they can provide qualitative/quantitative information in spray. The peak velocity magnitude in a spray plane measured by phase Doppler interferometry (PDI) represented plume direction along the injection duration [19]. The plume direction derived by the PDI measurement, was in good agreement with the data collected from the diffused back illumination extinction imaging (DBIEI). The plume direction also can be identified by planar laser imaging. However, quantification of the spray is not straightforward because of light scattering issue [20]. Another promising approach to acquire spray pattern is computed tomography using line-of-sight extinction imaging [21]. X-rays are able to penetrate dense media so it can be utilized for near nozzle plume detection where multiple scattering occur. A recent study showed that a commercial optical patternator (SETscan AP400) using line-of-sight imaging was also effective to detect plume collapse under flash-boiling conditions [22].

Despite these efforts, the identification of the plume direction under engine-like condition still remains as a challenge in regard to temporal and spatial resolution. The techniques described above have limitations in terms of complexity in measurement, high-cost in measuring equipment, laborious measurement procedures, and confined measurement domain. Therefore, in this study, a new 3-D tomographic reconstruction method was developed which can cover the entire spray domain and injection period with a much simpler setup. High-speed DBIEI and Mie-scattering imaging were performed in a constant flow vessel using the Engine Combustion Network (ECN) spray G injector. The primary objective of this work is to understand plume direction of the single component fuel iso-octane, the multi-component fuel diisobutylene, and olefinic fuels under various ambient conditions. This work also aims to provide high-fidelity experimental data for computational fluid dynamic (CFD) simulations.

Experimental setup

A series of spray test was carried out in a constant flow spray vessel. Real air motion present in engines such as swirl, tumble, and turbulent flow is hard to be simulated in the vessel, however, the constant flow spray vessel system has many advantages over optical engines: 1) Thermodynamic parameters can be controlled independently in the vessel system. Analysis of spray process at known boundary conditions is helpful to understand the effects of each thermodynamic parameter on spray characteristic and facilitate spray modelling. 2) The vessel system has a higher repetition rate than optical engines. In optical engines, spray imaging cannot be repeated many times in a short period due to the limitation of lubrication and thermal loading. Meanwhile, continuous spray imaging can be performed in a constant flow vessel. A reliable experimental data set can be provided and utilized as a validation source for modelling work. 3) Vessel system has much larger optical access than optical engines. In optical engines, the viewing area is limited to a portion of piston or piston liner. On the other hand, full optical access is available in the vessel. This feature facilitates simultaneous imaging for different views and advanced diagnostics using a laser system. 4) There is less impingement in the spray vessel than in optical engines. The spray in optical engines can create wetting on the cylinder wall or piston depending on the ambient condition due to limited space in the combustion chamber. On the contrary, the vessel has much more spacious volume so entire spray process can be recorded without wall impingement.

The schematic of the constant flow spray vessel is presented in Figure 1. The vessel was manufactured with stainless steel (2205) to withstand high pressure and temperature. The maximum operating temperature and pressure are 150 bar and 1300°C, respectively. The sprays were injected into a continuous nitrogen flow controlled by an electro-pneumatic flow controller (TESCOM,

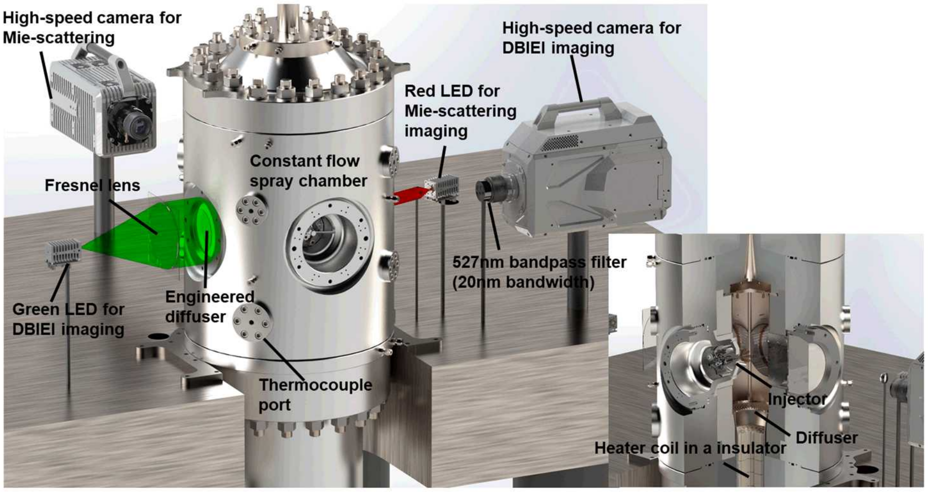

Figure 1. Experimental setup for high-speed Mie-scattering and DBIEI imaging (left: overall setup, right: cross cut image of the vessel).

ER5000). The continuous nitrogen flow rate was measured by a flow meter (BROOKS, 3809G) at the upstream of the vessel, and the exhaust flow was also measured by a flow meter (Alicat, MQ-2000SLPM-D/5M) at the exhaust pipe. The vessel pressure was measured by three different pressure transducers (WIKA, A10 and OMEGA PX119) at the vessel inlet. The heating coil surrounded by an insulator piece at the bottom part of the vessel was controlled by a temperature controller (Eurotherm, 3504). The flow after the heating coil went through a diffuser to enhance uniformity in the temperature field. Three layers which has total of 24 thermocouples were installed just above the diffuser, under the spray, and above the spray to monitor temperature distribution during the spray events. The fuel was injected when the average temperature of the spray center region reached a target ambient temperature. The mixture of injected fuel and nitrogen flow through the exhaust pipe at the top of the vessel. The vessel has an injector port and three optical windows, and was designed to have water cooling jackets in the wall, exhaust pipe, and window ports so the surface of the vessel could reside at room temperature even under high temperature conditions. The sprays were injected by an Engine Combustion Network (ECN) Spray G injector (Primary injector serial number: AV67-028). The Spray G injector is a solenoid driven gasoline direct injector which has nominally axisymmetric eight-holes. The inner nozzles were designed to have a diameter of 165µm with a counter bore diameter of 388µm. The nozzles were drilled with an angle of 37° from the center of the nozzle tip. Detailed dimensions and specifications are presented in Figure 2 and Table 1 [23].

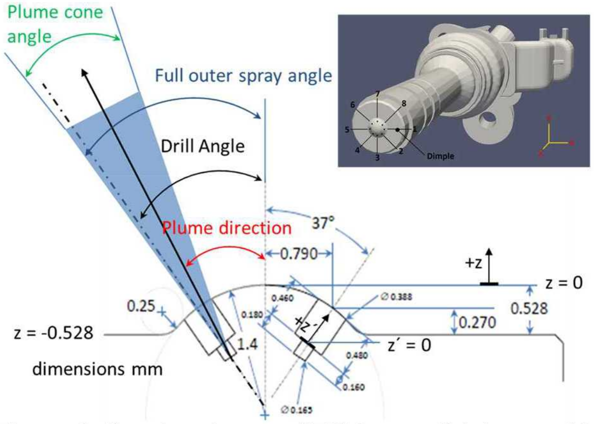

Figure 2. Cut plane image of ECN spray G injector with important dimensions (upper right shows 3-D rendering of the injector with primary orientation) [24].

The standard ECN electronic injector driver was utilized to have consistent injection and hold an injection profile similar with previous studies. A short electronic injection command of 680µs was delivered by an external data acquisition system (National Instruments, USB-6356). The injector tip temperature was monitored and maintained at 90°C by a water circulator (NESLAB, RTE111). The fuel was delivered by a dual-syringe pump system (Teledyne, D-series Model 65HP) with a fuel pressure of 200 bar. The volume of the syringe pump fuel system is much smaller than a fuel system which consisted of a massive high pressure fuel pump and rail so a lot of fuel could be saved during fuel change and flushing process. Quartz windows with 130mm diameter were installed at the three remaining ports in the vessel. They provided optical access for DBIEI line-of-sight imaging through the side windows and for Mie-scattering imaging to the front of the injector.

Parameters	**Level**
Number of holes	8
Spray shape	Circular
Orifice diameter	165µm
Step diameter	388µm
Hole shape	Straight
Orifice drill angle	37°
Full outer spray angle	80°

Table 1. Specifications of ECN Spray G injector [24].

The liquid phase fuel was visualized by DBIEI technique. A high-speed green light emitting diodes (LED) Fresnel lens (150mm, f=150mm), engineered diffuser (20°), and band pass filter (center wavelength: 527nm, bandwidth: 20nm, full width-half max: 22nm) were utilized for the imaging. A high-speed digital video camera (Photron, SA-Z) equipped with a prime lens (Nikkor, 50mm f/1.8) was used to capture images of spray development in the vessel. The green LED was operated with 24ns command signal width to freeze the spray in the frame. The imaging was performed at a shutter speed of 67,200 frames per second (fps) with an image resolution of 512 by 512. The aperture of lens and exposure time of the high-speed camera were set to 2.8 and 13.27µs, respectively. The LED light was operated 7µs after the shutter opening to be placed in the middle of shutter opening period. The recording was extended up to 5ms after the start of injection (SOI) to capture entire spray development and evaporation process. The Mie-scattering signal illuminated by the red LED was also recorded by a high-speed camera (Phantom, v311) with a prime lens (Nikkor, 50mm f/1.8). The images were taken with an exposure time of 39.4µs and a frame rate of 25,000 with a resolution of 304 by 304. The signal duration for LED and f stop of the lens were set to 1ms and 4, respectively. The DBIEI imaging provided quantitative liquid distribution in the spray, meanwhile, Mie-scattering facilitated detection of plume-to-plume interaction from the front view. The temperature distribution, oxygen concentration, and vessel pressure were acquired by a DAQ system (National Instruments, NI-9214 and NI-9202).

Test fuels

Single component fuel iso-octane, multi-component surrogate diisobutylene, and multi-component fuel with olefin molecular structure were tested in the spray vessel. The iso-octane, which was widely investigated in ECN work, was selected as a base fuel. The other two fuels were considered as promising alternative fuels for gasoline because they have similar fuel properties with conventional gasoline and they can be produced from renewable resources. All of three fuels had research octane number (RON) of 92. Figure 3 presents the vapor pressure of three fuels according to temperature. The vapor pressure of diisobutylene was not available but replaced by Alkylate fuel which was expected to be similar with diisobutylene. The olefinic fuel showed the highest vapor pressure followed by Alkylate and iso-octane. This implies the olefinic fuel has a higher chance of flash-boiling at a certain ambient pressure condition because of the lower pressure ratio (ambient pressure to saturation pressure).

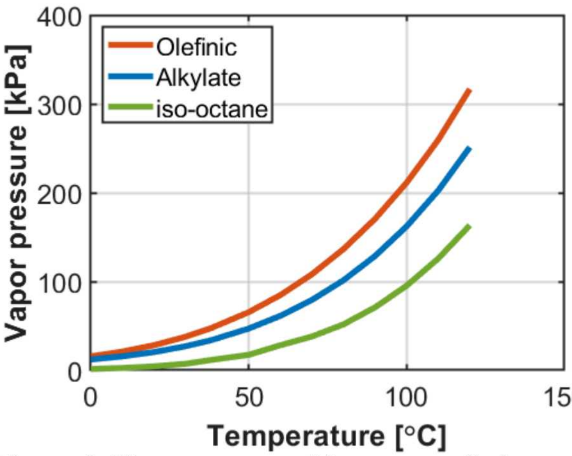

Figure 3. Vapor pressure of iso-octane, alkylate, and olefinic fuels [24].

The distillation curve of tested fuels is shown in Figure 4. The iso-octane, a single component, showed a flat line which represented its boiling temperature. The pseudo distillation curve of diisobutylene which composed of five different species; hexane (4% v/v), heptane (12.1% v/v), iso-octane (44.2% v/v), toluene (20.1% v/v), and diisobutylene (19.6% v/v) was derived from the boiling point of each component. It also shows a flat distillation curve around 100°C similar to iso-octane. The olefinic fuel has a wide-range distillate that covers 50˚C to 200˚C. This means the olefinic fuel contains not only light volatile components but also heavy components which are hard to evaporate out of fuel. The distillation curve of olefinic fuel was closest to gasoline fuel for real engine application.

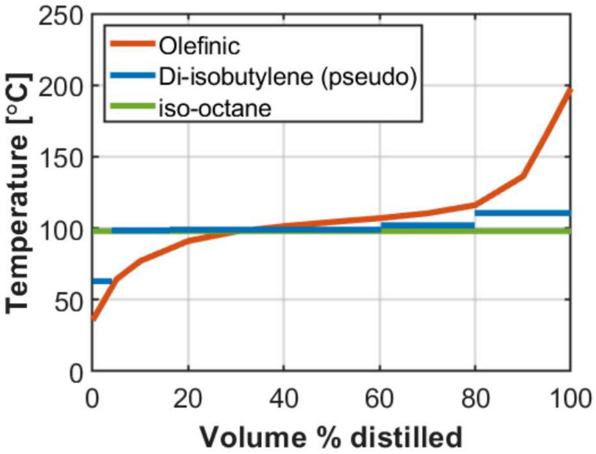

Figure 4. Distillation curve of iso-octane, alkylate, and olefinic fuels (Test method ASTM D86) [24].

Tomographic reconstruction procedure

The tomographic reconstruction process starts from a projected liquid volume (PLV) calculation. First of all, spray images of 300 injections were ensemble averaged. In this step, floating counts in the CMOS sensor of high-speed camera were rejected by subtracting averaged counts in each frames. The instantaneous images of spray were converted to optical thickness using following equation.

$$\tau = -\ln(I/I_o) \quad (1)$$

where I is an image with spray and I_o is an averaged image of background without spray. The projected liquid volume could be calculated using Mie-scatter extinction theory which is presented by following equation.

$$\tau \frac{\pi d^3/6}{C_{ext}} = \int_{-y_\infty}^{y_\infty} (Liquid\ volume\ fraction) \cdot dy \quad (2)$$

where d is droplet diameter, C_{ext} is the extinction coefficient decided by optics setup in the experiment, and LVF is the liquid volume fraction. In this study, 7μm and $78.77 \cdot 10^{-6}$ were used for d and C_{ext}, respectively [24]. The spray boundary was determined with an ECN recommended projected liquid volume threshold of $0.2 \cdot 10^{-3}$mm^3(liquid)/mm^2 to measure liquid penetration length and spray width. The liquid penetration length was defined as the t axial distance from the nozzle to the spray boundary in the primary view. The spray width was measured at 15mm and 25mm from the nozzle tip. Tomographic reconstruction needs spray imaging at different view so spray data in three different views was acquired. The injector adaptor was rotated to get 0° (ECN primary), 11.25°, and 22.5° (ECN secondary) view on spray. Line data at a certain plane (a certain distance from the nozzle tip) can be extracted. The data of full map from 0° to 180° was successfully achieved by interpolation/extrapolation using line data from each view. Finally, the foot print of the spray at a certain plane was created by stacking data planes. The tomographically reconstructed data was validated with an experimental result from Delphi. There was some level of discrepancy especially with plumes 1,4, and 5. However, the averaged plume direction angles were very close. It showed only 0.01° difference between tomographically reconstructed data and measurement.

Experimental conditions

The spray experiments were carried out under ECN Spray G2, G3, and G3HT (G3 with elevated temperature conditions). Those conditions represent early intake injection. The fuels were injected by ECN Spray G injector with a 200 bar injection pressure. An electronic command with a duration of 680μs (780μs actual fydraulic duration) was delivered to inject 10mg of fuel in the vessel. The injector tip temperature was kept at 90°C for the duration of experiments. The ambient temperature was set to 60°C for G2 and G3 condition, but increased to 120 °C under G3HT condition. The ambient pressures were 0.5 bar, 1 bar, and 1.18 bar for G2, G3, and G3 HT, respectively. Corresponding ambient densities were 0.5 kg/m^3 for G2, 1.12 kg/m^3 for G3 and G3HT conditions.

Effect of ambient conditions on plume direction

Line-of-sight measurements with iso-octane fuel was compared under G2, G3, and G3HT conditions. Figure 5 presents spray outlines, liquid length, and liquid width at different conditions. Vertical lines in the outline images show the liquid penetration length of the spray. The spray outline differentiates the liquid fuel region in the mixture. The spray under G3HT condition shows much faster evaporation than G2 and G3 conditions. This is as expected because of higher ambient temperature. The liquid phase spray was completely evaporated approximately at 2ms after SOI. Downstream of the spray under G3HT condition showed much narrower liquid width than other fuels. However, the liquid width at near nozzle did not show noticeable difference than G2 condition. This is because diffusion along the radial direction compensated liquid extinction by evaporation. Meanwhile, the liquid length under G3HT condition showed a very similar trend to G3 condition because of identical ambient density. The liquid length got smaller after SOI when the sprays lost their momentum but evaporation was still occurring. The spray under G2 condition showed the longest liquid length due to the lowest ambient density. However, the liquid width had a similar level

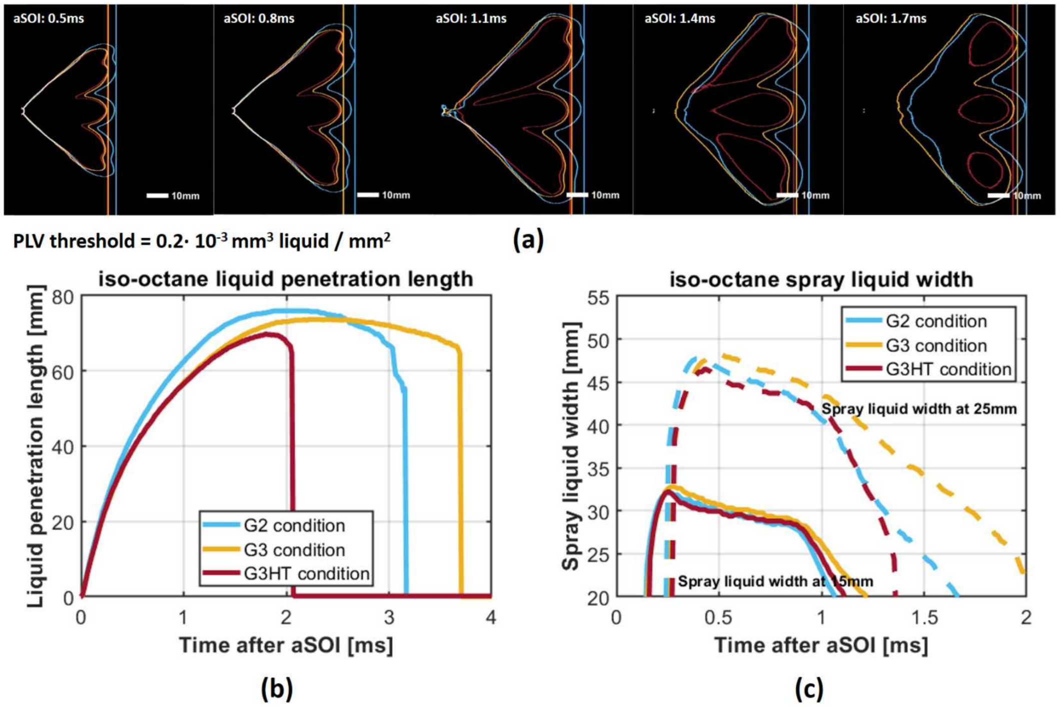

Figure 5. Line-of-sight results of (a) projected liquid volume outline (the outline was determined by using a threshold of 0.2· 10^{-3} mm^3 liquid / mm^2, (b) liquid penetration length, and (c) liquid width at 15mm, and 25mm.

to the G3HT condition. It seems that slight spray collapse occurred under flash-boiling condition showing smaller near nozzle liquid width under G2 condition. The liquid did not persist as long as G3 condition but time for complete evaporation took over 3ms. A thermodynamic analyses based on the first law was carried out to understand physical background of long liquid residual time. The liquid fuel and air were assumed to form a homogeneous mixture. The calculation result in Figure 6 shows how much liquid can be completely evaporated into vapor phase. The initial ambient (333K for G2 and G3 conditions, 363K for G3HT condition) and fuel(363K) temperatures are presented in the graph.

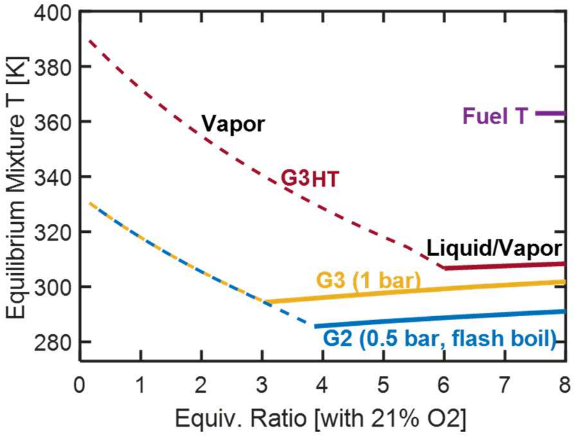

Figure 6. A thermodynamic analysis on fuel evaporation depending on ambient condition.

The graph indicates that the final mixture temperature decreased as the liquid absorbed heat from the ambient air to change phase. The temperature drop got larger as the initial liquid fuel mass increased, for example, temperature drop at equivalence ratio of 3 is much greater when compared to the case under equivalence ratio of 1. In terms of ambient conditions, G2 and G3 had a much lower equivalence ratio limit than the G3HT condition. This implies that G3HT condition has larger capability of complete evaporation due to the elevated ambient temperature. Under fuel rich condition, fuel can be remained as liquid phase because of the excessive cooling from the phase change and this is finally resulted in a long residual time as shown in Figure 5.

Tomographic reconstruction enabled a comparison of mixture quality at any plane. Outlines of liquid volume fraction with a threshold of $5 \cdot 10^{-3}$ are presented in Figure 7. It is noted that this is not line-of-sight data but Y-Z plane information in a three dimensional space. The macroscopic spray characteristics which are confirmed in the line-of-sight result also can be seen in this image. The G3HT spray evaporated much faster than other cases showing a smaller spray area. The longest liquid length under G2 condition is also consistent with previous discussion. The merit of tomographic data is that accurate plume direction can be identified. The nozzle drilling angle is indicated as a red dotted line which forms a 37^{o} from Z axis. As compared to this reference angle, the real plume direction angle was approximately 4^{o} smaller regardless of ambient conditions. Another interesting feature is that the leading edge has a memory of the first plume direction angle. The sprays moved outward showing the curved shape as plume direction angle in the near nozzle area decreased. To compare spray behavior, the plume direction angle was calculated based on an averaged liquid volume fraction in the radial direction. The angle between the nozzle hole and a middle point at 75% of maximum liquid volume fraction defined plume direction angle. Figure 8 shows the plume direction angle calculated at a 30mm plane from the nozzle (Z=30mm). The Mie-scattering images are also presented at the top.

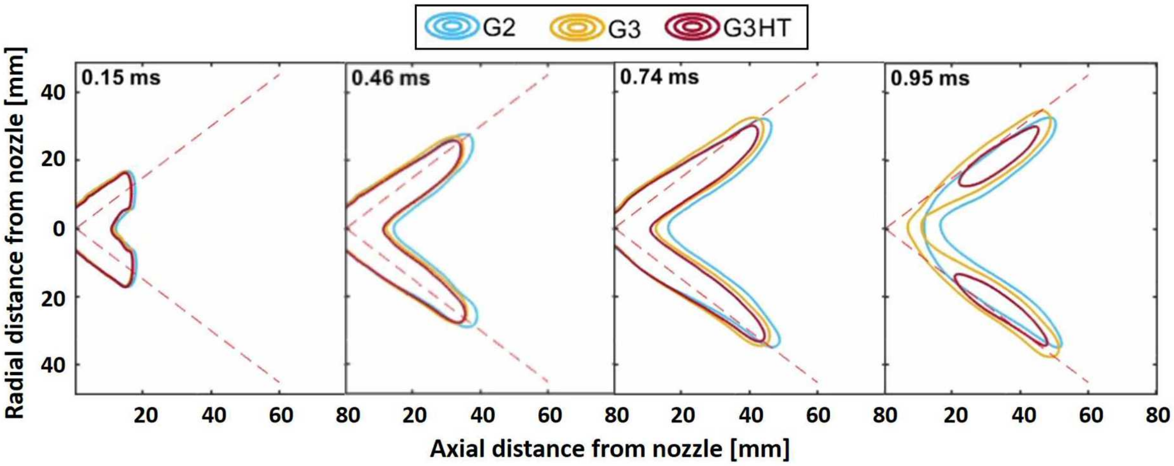

Figure 7. Comparison of liquid volume fraction outline with a threshold of $5 \cdot 10^{-3}$ under three different conditions using iso-octane (the data from 3-D tomographic reconstruction).

It shows the plume direction angle is decreasing during the injection period. It decreased 2^o at the end of injection when compared to SOI for G3 and G3HT conditions. The G2 condition showed a much larger decrease in the plume direction angle. This plume collapse is attributed to the plume-to-plume interaction as shown in the Mie-scattering images. The spray plume under G2 condition showed a wider plume width than the G3 condition due to flash-boiling. This plume-to-plume interaction is most likely altered the velocity and pressure field in the spray to induce spray collapse.

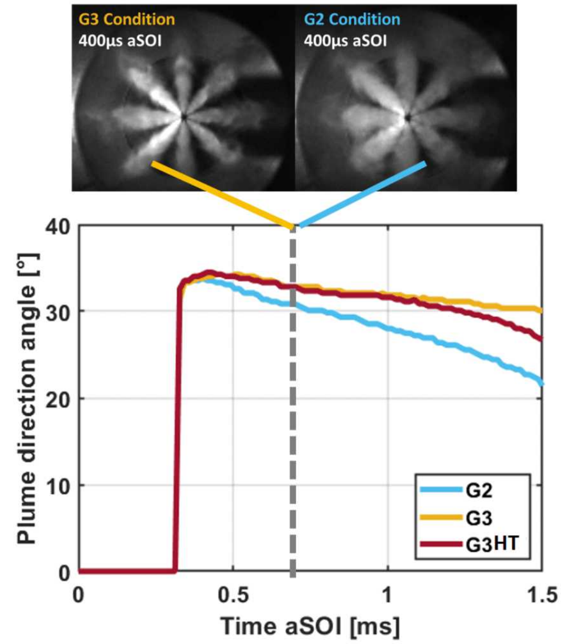

Figure 8. Calculated plume direction angles with iso-octane under G2, G3, and G3HT conditions (upper figures show more plume-to-plume interaction under G2 condition).

The plume collapse can be clearly seen with an averaged liquid volume fraction at Z=30mm plane. Figure 9 shows the liquid volume fraction profiles at 0.5ms and 1ms after SOI. As confirmed in Figure 7, there is no distinct difference in the peak location between G3 and G3HT condition. However, the peak of the liquid volume fraction explains the evaporation characteristics well. The G3 condition indicated the highest peak of the liquid volume fraction due to the less evaporation while G3HT showed the lowest peak of the liquid volume fraction. The overall liquid volume fraction curve under G2 condition moved to the center of the spray as plume collapse occurred. The peak of the liquid volume fraction under G2 condition was translated approximately 4mm from its initial peak location. Meanwhile, G3 and G3HT condition showed 1mm movement toward center. This implies that plume collapse under G2 condition was more severe than other cases.

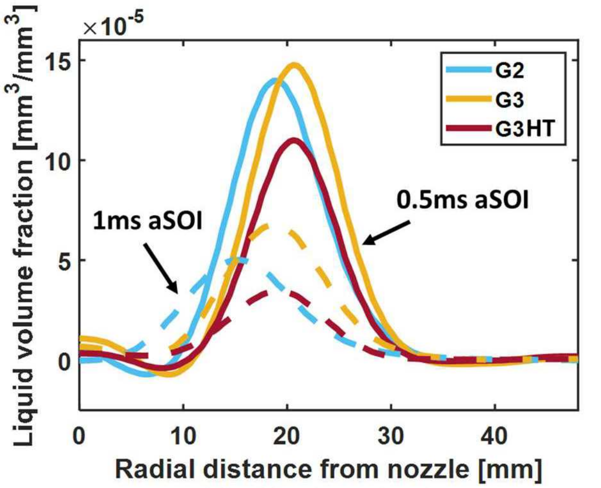

Figure 9. Averaged liquid volume fraction at Z=30mm. The solid lines present 0.5ms after SOI and dot lines show 1ms after SOI.

Effect of fuels on plume direction

The outline of liquid phase fuel, liquid length, and liquid width derived from line-of-sight projected liquid volume measurement under G2 condition are shown in Figure 10. The diisobutylene had slightly a longer liquid penetration length and a wider liquid width than iso-octane. Light components in the diisobutylene could have resulted in the wider liquid width because of the earlier start of evaporation when compared to iso-octane. At the same time, the heavy species such as heptane and toluen need a longer time to be evaporated thus it showed longer liquid penetration length than iso-octane. The distinct difference in macroscopic spray characteristics can be seen in the olefinic fuel case. It showed the shortest liquid penetration length and a narrower liquid width at 15mm than the other fuels. The olefinic fuel is a wide range distillate which contains not only light components but also heavy species as shown in the distillation curve (refer Figure 4). The consecutive images of the spray outline indicate that there was a strong spray collapse using olefinic fuel which showed a much narrower liquid width at the near nozzle region. The collapsing spray delivered its momentum mainly in the core area so the liquid penetration length increased again from 2.5ms after SOI. The olefinic fuel also had the largest spray width at 25mm because the leading spray was dispersing in a radial direction by the dense mixture in the core area. In terms of residual time, diisobutylene evaporated approximately 2.5ms which is 0.7ms shorter than iso-octane. The olefinic fuel showed the longest residual time of 4.9ms. This time scale is enough to cause wall wetting in engines.

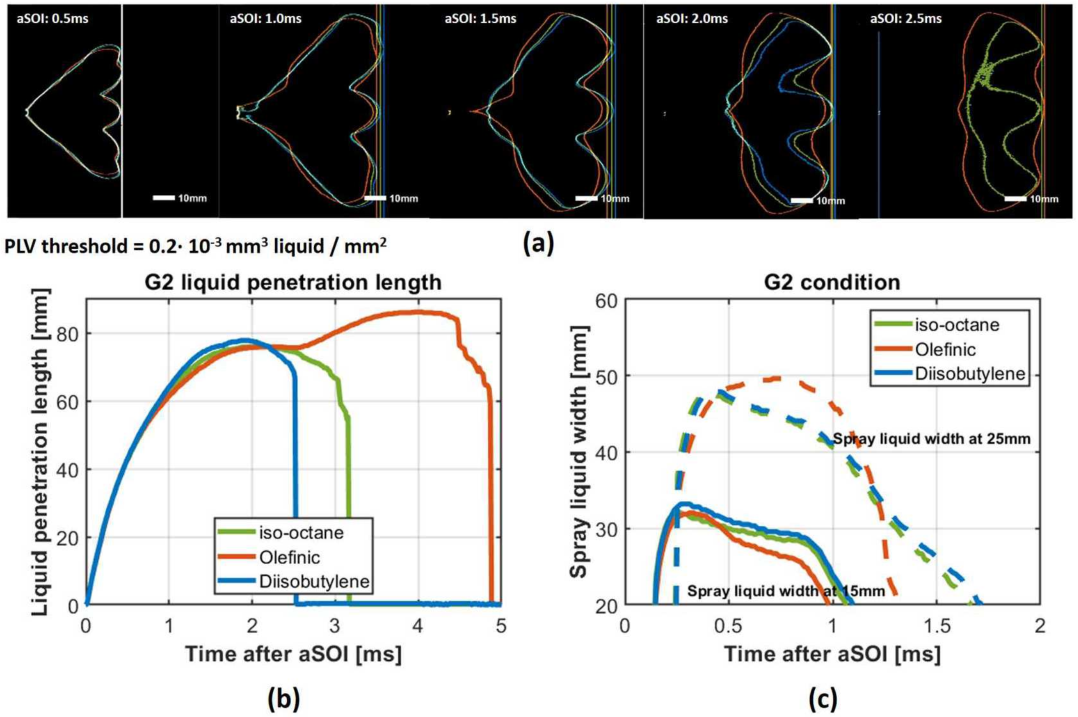

Figure 10. Line-of-sight results of (a) projected liquid volume outline (the outline was determined by using a threshold of $0.2\cdot 10^{-3}$ mm^3 liquid / mm^2, (b) liquid penetration length, and (c) liquid width at 15mm, and 25mm with different fuels under G2 condition.

Even though the olefinic fuel showed a strong plume collapse in the near nozzle region due to the light components, the heavy species remained for a long time to be evaporated.

The liquid volume fraction contour in the Y-Z plane is presented in Figure 11. The outline was defined with a threshold of $5\cdot 10^{-3}$. The slightly longer liquid penetration length and wider liquid width of diisobutylene can be seen in the spray outline. Again, all three plumes penetrated with a smaller plume direction angle than the nozzle drilling angle (37°). Especially for olefinic fuel, the vigorous spray collapse occurred starting at 10mm, creating a liquid fuel mixture in the core region. This fuel rich mixture slowly moved forward and remained much longer than iso-octane and diisobutylene fuels.

The plume direction angle and Mie-scattering images are shown in Figure 12. In the line-of-sight result, the liquid width of diisobutylene was larger than that of iso-octane. However, the plume direction angle of diisobutylene is slightly narrower than iso-octane. This implies that the diisobutylene might had more plume-to-plume interaction than iso-octane because of the wider

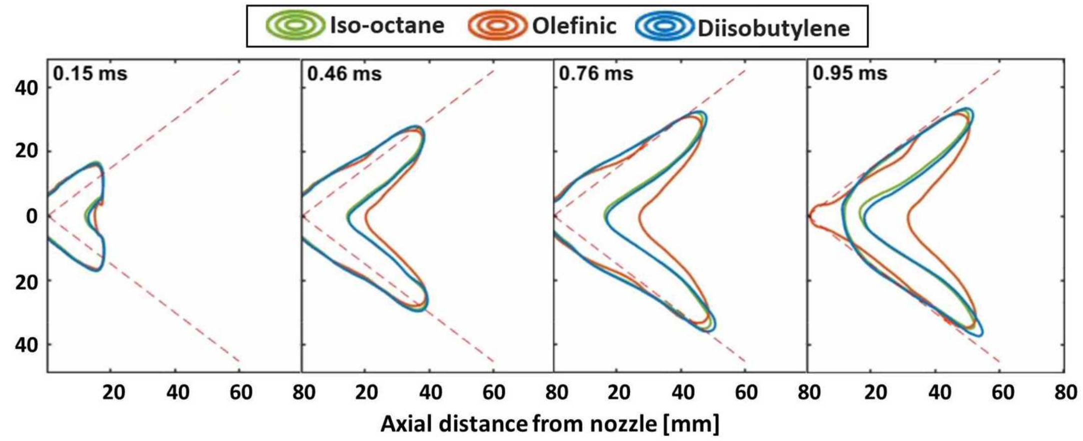

Figure 11. Comparison of liquid volume fraction outline with a threshold of $5\cdot 10^{-3}$ under G2 condition using different fuels (the data from 3-D tomographic reconstruction).

plume width. The vigorous plume collapse with olefinic fuel can be seen in the Mie-scattering image. The boundary between plumes are not clear near the nozzle region, however, each of plumes downstream could be identified. Plume direction angle of olefinic fuel dropped sharply after plume collapse occurred. The difference in plume direction angle between olefinic fuel and other fuels was approximately 3^o at the beginning, however, it increased more than 10^o after 1ms after SOI. The plume collapse of olefinic fuel drastically modified the mixture distribution.

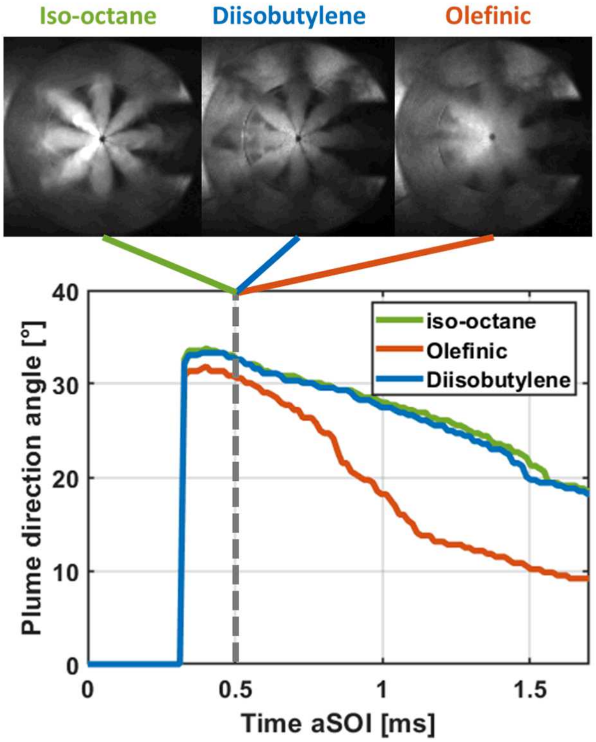

Figure 12. Comparison of plume direction angles of three different fuels under G2 condition (upper figures show vigorous plume collapse with olefinic fuel).

The averaged liquid volume fraction at Z=30mm under G2 condition is shown in figure 13. The peaks of the liquid volume fraction translated toward center due to spray collapse regardless of fuels. The peak of the liquid volume fraction with diisobutylene was slightly more toward center of the spray than iso-octane. The liquid volume fractions with iso-octane and diisobutylene decreased as evaporation occurred, however, olefinic fuel maintained a significant amount of liquid during plume collapse.

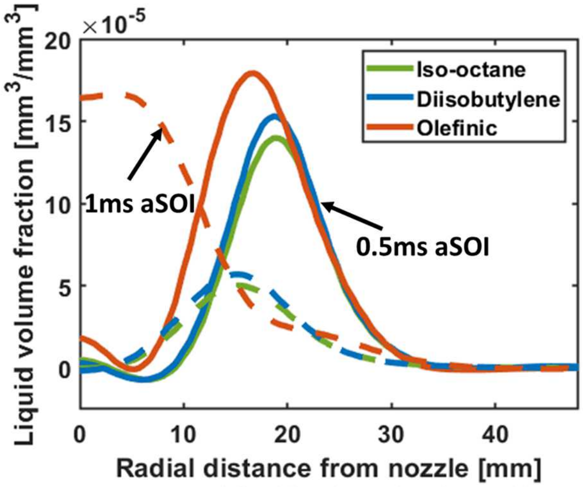

Figure 13. Averaged liquid volume fractions of iso-octane, diisobutylene, and olefinic fuels at Z=30mm (solid lines indicate 0.5ms aSOI and the dot lines show 1ms aSOI).

Conclusion

In this study, we developed a technique to measure the plume direction using 3D tomographic reconstruction from a line-of-sight projected liquid volume measurement. The new processing routine was applied under G2, G3, and G3HT conditions with iso-octane, diisobutylene, and olefinic fuel in a constant flow spray vessel. The experimental results showed that G3HT condition had a shorter liquid penetration length and a narrower liquid with when compared to G2 and G3 conditions due to having a higher ambient temperature. A slight plume collapse under G2 condition resulted in the longest liquid length. A significant amount of liquid was detected under all ambient conditions due to vaporization cooling and a lack of mixing-limited behavior. Based on the reconstruction result, there was an approximately 4^o smaller plume direction angle than the nozzle drilling angle regardless of ambient conditions. Plume collapse under the G2 condition had a narrower plume direction angle than both the G3 and G3HT conditions. In terms of fuels, diisobutylene showed slightly longer liquid penetration length and a wider spray width than iso-octane. The light components in the olefinic fuel attributed to the plume collapse and a narrower near nozzle liquid width. Meanwhile, heavy species in the olefinic fuel attributed to the longest residual time. Complete evaporation took almost 5ms, which is long enough to make contact with the piston or cylinder in an engine.

References

1. Hoffman, G., Befrui, B., Bernforfer, A., Piock, W.F., Varble, D.L., SAE International Journal Engines 7:519-527 (2014).
2. Park C., Kim S., Kim H., Moriyoshi, Y., Energy 41:401-407 (2012).

3. Costa, M., Sorge, U, Merola, S., Irimescu, A., Villetta, M.L., Rocco, V., Energy 117:405-415 (2016).
4. Yang, J., Dong, X., Wu, Q., Xu, M., Applied Energy 236:137-146 (2019).
5. Dernotte, J., Dec, J., Ji, C., SAE Technical Paper 2017-01-0728 (2017).
6. Stuhldreher, M., Kargul, J., Berba, D., McDonald, J., Bohac, S., Dekraker, P., Moskalik, A., SAE International Journal Engines 11:1273-1305 (2018).
7. Luijten, B., Somers, B., Adomeit, P., Brumm A., SAE Technical Paper 2013-01-1604 (2013).
8. Xu, M., Zhang, Y., Zeng, W., Zhang, G., Zhang, M., SAE International Journal of Fuels and Lubricants 6:137-148 (2013).
9. Postrioti, L., Bosi, M., Cavicchi, A., Abuzahra, F., Gioia, R.D., Bonandrini, G., SAE Technical Paper 2015-24-2480 (2015).
10. Zhang, G., Hung, D.L.S., Experiments in Fluid 55:1804 (2014).
11. Zhang, M., Xu, Min, Hung, D.L.S., Measurement Science and Technology 25:095204 (2014).
12. Zheng, W., Xu, Min, Zhang, G., Zhang, Y., Cleary D.J., Fuel 95:287-297 (2012).
13. Sphicas, P., Pickett, L.M., Skeen, S., Frank, J., International Journal of Engine Research 19:1048-1067, 2018.
14. Serras-Pereira, J., Romunde, Z.V., Aleiferis, P.G., Richardson, D., Wallace, S., Cracknell, R.F., Fuel 89:2592-2607 (2010).
15. Kale, R., Banerjee, R., Fuel 236:1-12 (2019).
16. Chen, Y., Zhang, Y., Cheng W.K., SAE Technical Paper 2018-01-0360 (2018).
17. Li Y., Guo, H., Zhou, Z., Zhang, Z., Ma, X., Chen, L., Fuel 236:677-685 (2019).
18. Parrish, S., SAE International Journal Engines 7:1017-1033 (2014).
19. Duke D.J., Kastengren, A.L., Matusik, K.E., Swantek, A.B., Powell, C.F., Payri, R., Vaquerizo, D., Itani, L., Bruneaux, G., Grober, R.O., Parrish, S., Markle, L., Schmidt, D. Manin, J., Skeen, S.A., Pickett, L.M., Experimental Thermal and Fluid Science 88:608-621 (2017).
20. Berrocal, E., Kristensson, E., Richter, M., Linne, M., Alden, M., Optics Express 16:17873 (2008).
21. Pickett, L.M., Manin, J., Kastengren, A., Powell, C., SAE International Journal Engines 7:1044-1053 (2014).
22. Parrish, S., Zink, R.J., Sivathanu, Y., Lim, J., 22th International Conference on Liquid Atomization and Spray Systems, Cincinnati, Ohio, May 2010, pp. 16-19.
23. Engine Combustion Network webpage [www.ecn.sandia.gov].
24. Fouts, L., Fioroni, G.M., Christensen, E., Ratcliff, M., McCormick, R.L., Zigler, B.T., Sluder, S., Szybist J.P., Dec, J.E., Miles, P.C., Ciatti, S., Bays, J.T., Pitz, W., Mehl, M, "Properties of Co-Optima Core Research Gasoline", National Renewable Energy Lab. (NREL), Report No. NREL/TP-5400-71341.

Contact information

Lyle M. Pickett
LMPicke@sandia.gov

Nomenclature

C_{ext}	extinction coefficient
d	droplet diameter
I	instantaneous spray image
I_o	averaged background image
τ	optical thickness

Acknowledgement

The authors would like to thank Tim Gilbertson, Alberto Garcia, Brian Patterson, Keith Penny, Nathan Harry, Aaron Cyzenski, Chris Ingwerson, Laurie Bell, Paul Abers, Pater Cable for their dedicated support for the research facility.

The work was performed at the Combustion Research Facility, Sandia National Laboratories, Livermore, CA. This research was conducted as part of the Co-Optimization of Fuels & Engines (Co-Optima) project sponsored by the U.S. Department of Energy (DOE) Office of Energy Efficiency and Renewable Energy (EERE), Bioenergy Technologies and Vehicle Technologies Offices. Sandia National Laboratories is a multimission laboratory managed and operated by National Technology and Engineering Solutions of Sandia, LLC., a wholly owned subsidiary of Honeywell International, Inc., for the U.S. Department of Energy's National Nuclear Security Administration under contract DE-NA0003525